

The Effects of Clumping on Derived Abundances in H II Regions

John S. Mathis¹ and Kenneth Wood²,

¹*Astronomy Department, University of Wisconsin,*

475 N. Charter Street, Madison, WI 53706; mathis@astro.wisc.edu

jmailto:mathis@astro.wisc.edu ²*School of Physics & Astronomy, University of St. Andrews,*

North Haugh, St Andrews, KY16 9SS, Scotland; kw25@st-andrews.ac.uk jmailto:kw25@st-andrews.ac.uk jmailto:kw25@st-andrews.ac.uk

Released 2004 Xxxxx XX

ABSTRACT

We have compared Monte Carlo photoionization models of H II regions with a uniform density distribution with models with the same central stars and chemical compositions but with 3-D hierarchical density distribution consisting of clumps within clumps, on a four-tier scheme. The purpose is to compare the abundances of He, N, O, Ne, and S obtained by standard analyses (emission line strengths and measured mean temperatures from [O III] and [N II]) to the abundances in our models. We consider stellar temperatures in the range 37.5 – 45kK and ionizing photon luminosities from $10^{48} - 10^{51} \text{ s}^{-1}$.

Clumped models have different ionic abundances than uniform. For hot stars, (He^0/H^+) is 2 – 3%, much larger than with uniform models. This amount of He^0 is independent of metallicity and so impacts the determination of the primordial abundance of He. The total abundances of O, Ne, and S obtained by the usual methods of analysis, using $T([\text{O III}])$ for high stages of ionization and $T([\text{N II}])$ for low, are about as accurate for clumped models as for uniform and within $\sim 20\%$ of the true values. If $T([\text{O III}])$ is used for analyzing all ions, the derived (O/H) is $\sim 40 - 60\%$ too large for cool stars but is good for hot stars. Uniform models have similar errors, so the clumping does not change the accuracy of abundance analysis.

The physical causes of the ionic abundance errors are present in real nebulae. In clumped models, helium ionizing radiation from zones of high ionization (low He^0 and low UV opacity) can penetrate nearby regions near the edge of the ionized zone. This effect allows He^0 to absorb more stellar photons than in uniform or radially symmetrical geometries. In turn, these absorptions compete with O^+ , etc., for those energetic stellar photons.

Key words: radiative transfer — ISM — H II regions — cosmology

1 INTRODUCTION

The interstellar medium (ISM) has filamentary structure over scales ranging from hundreds of parsecs through AUs. This paper will analyze some of the properties of H II regions formed by ionization of the clumpy interstellar gas and compare them to those produced by the same code for models with a spatially uniform density. The Monte Carlo photoionization code (Wood et al. 2004) treats gas with densities that have a power-law or scale-independent character over about an order of magnitude in spatial sizes (see §2). We refer to these hierarchical models as “clumped”.

Our goal is to isolate the effects of clumping by comparing clumped models with smooth density distributions, while keeping other important parameters (e.g., the stel-

lar atmospheres and luminosities that strongly influence the nebular models, and the nebular composition) constant. We choose the other parameters rather arbitrarily and do not try to compare our models with real objects. Several types of questions motivate us:

(a.) For a fixed exciting star and mean nebular density, how are the ionization and temperature structures of the resulting ionized nebulae affected? What are the physical causes of the differences? How do the differences vary as the nebular parameters (e.g., exciting star properties, geometry of the clumps, and the mean gas density) are changed?

(b.) How accurately are model ionic abundances determined from the emission lines, using techniques similar to those commonly used to analyze observations of real nebu-

arXiv:astro-ph/0503577v1 26 Mar 2005

lae? What errors occur in the ionic abundances derived from ratios of fluxes of emission lines, using mean nebular electron temperatures, T_e , estimated from diagnostic line ratios?

We assume idealized conditions, neglecting observational errors and reddening of emission lines by interstellar dust either within or exterior to the H II region. Thus, our abundance errors are lower limits to those expected for real nebulae. We consider the effects of dust in the transfer of Lyman continuum radiation within the ionized gas.

Our assumptions and the limits of parameter space that we explored are given in §2. In §3 we consider the physical differences among the clumped models and their differences from uniform models. In §4, we discuss the relevance of our models to real nebulae and the uncertainties of abundances within them.

We do not address the important issue of differences in abundances of many ions derived from recombination lines as opposed to collisionally excited lines. A common explanation is that there are “anomalous” temperature variations within the ionized plasma (see, e.g., García-Rojas et al. 2004, and references therein), although the phenomenon seems more complicated (e.g., Tsamis et al. 2003). We have used only standard physics, and our abundances from recombination lines would be almost the same as from collisionally excited lines.

2 ASSUMPTIONS USED IN THE MODELS

There are many free parameters that affect the spectrum and abundances derived from model H II regions, and we consider only a subset of possible parameter space. We make the following assumptions:

1. The models are in a steady state, thereby neglecting the dynamics occurring near the outer $H^+ \rightarrow H^0$ ionization front, where probably a D-type front (see, e.g., Osterbrock 1989) is propagating into the surrounding neutral material. This is the standard assumption in H II region models. However, the conditions near the ionization front are important for N^0 and O^0 , which are sensitive to the temperature and ionization structure at the outer edge of the ionized region.

2. We chose the composition used for workshops for testing model H II regions (Ferland et al. 1995, Péquignot, D., et al. 2001) : H, He, C, N, O, Ne, and S = 1, 0.1, $2.2 \cdot 10^{-4}$, $4.0 \cdot 10^{-5}$, $3.3 \cdot 10^{-4}$, $9.0 \cdot 10^{-6}$, and $5.0 \cdot 10^{-5}$, respectively, by number. These abundances are rather arbitrary, but are adequate for investigating the important physical effects introduced by clumping. We will refer to elemental abundances as chemical symbols without superscripts, so that (O/H) is the abundance ratio of O, including all stages of ionization, relative to H.

3. Dust in H II regions and within the diffuse ionized gas (DIG) needs careful consideration. We will show below that carbonaceous grain material has probably largely been converted to the gas phase. We will find that the effects of carbon-depleted dust are not very significant, but that with other assumptions dust could become dominant in determining the structure of the ionized region.

Dust affects the emitted nebular spectrum by reddening the nebular radiation and also by absorbing ionizing radiation. Since corrections for reddening are routinely made, we assume that line strengths are determined perfectly. This as-

sumption is very optimistic when we consider the spatially unresolved emission line fluxes rather than the pixel-by-pixel line intensities (see §3.2).

If there were no destruction of dust within the ionized zone, the absorption of ionizing radiation by dust would be hugely important, while dust scattering, strongly directed forward, has almost no effect. The absorption cross section of graphitic carbon, closely related to absorption by polycyclic aromatic hydrocarbons (PAHs), peaks at about 17 eV with a cross section of $3 \times 10^{-21} \text{ cm}^2 (\text{H atom})^{-1}$ according to the model of Weingartner & Draine (2001), with the cross sections conveniently tabulated in Draine (2004). This exceeds the opacity of H if $(H^0/H) \leq 0.001$, which occurs over most of the volume of the nebula. Dust with this carbonaceous cross sections absorbs $\sim 90\%$ of the ionizing radiation over our entire range of models, for all geometries. By contrast, the silicate component of dust is relatively gray in the ionizing UV, with an opacity of roughly $1.3 \times 10^{-22} \text{ cm}^2 \text{ H}^{-1}$, only 5% of the peak of carbonaceous dust.

The abundance of dust in H II regions can be estimated by means of the gas-phase abundances of refractory elements (e.g., C, Al, Mg, Ca, or Fe; see Savage & Sembach 1996) that are mostly locked up in dust in the diffuse ISM. Abundances found in bright H II regions are significantly different, especially for C. In the diffuse *neutral* ISM, the C II abundances derived from absorption towards 12 B stars is $C/H = 160 \pm 17$ ppM and an upper limit of 108 ppM for another (Sofia et al. 2004). In various H II regions, gas phase C/H varies from 330 to 590 ppM (Esteban et al. 2004a, Esteban et al. 1999a, Esteban et al. 1999b, García-Rojas et al. 2004). Solar $(C/H) = 245 \pm 30$ ppM (Asplund et al. 2005, Holweger 2001). Interstellar abundances have probably been significantly enhanced since the formation of the Sun, perhaps dex(0.2) to ~ 400 ppM (e.g., Ackerman et al. 2004, Pagel & Tautvaišienė 1995). The Orion Bar (Sellgren et al. 1990), an ionization front seen edge-on, shows $3.3 \mu\text{m}$ aromatic hydrocarbon emission arising from a rather thin zone between the $P\alpha$ and $Br\alpha$ recombination lines of H and emission lines of H_2 . Thus, several observations require that bright H II regions have most or almost all of their carbon in the gas phase. Usually H II regions have strong near-infrared emission bands, but it may be that the carriers are actually in the neutral gas adjacent to the ionized.

In some H II regions, siliceous dust is present within the ionized gas. In M17, only about 15% of the Fe is in the gas phase (Esteban et al. 1999b). Within the DIG, Howk & Savage (1999) found that Al III/S III is much less than solar. Both ions are found only in the gas in which H is ionized, so Al is depleted onto grains in the DIG. Further direct evidence for dust within the DIG is given by the correlation of the diffuse $H\alpha$ with $100 \mu\text{m}$ emission and the lack of correlation with HI (Lagache et al. 2000).

In summary, it seems that the carbonaceous component of dust has largely been vaporized in H II regions while the siliceous grains may largely remain intact. Perhaps processes that convert carbon in grains to the gas phase act very rapidly in ionized gas, so that the C in dust (including PAHs and the “very small grains,” carbonaceous in character) does not absorb ionizing radiation when H is mostly H^+ . Pure silicate dust has cross sections so low and so weakly dependent on wavelength that its presence is not crucial to

the results of this paper. We ran models that confirmed this statements, but for most models in this paper we neglected dust and also heating by PAHs.

4. Our algorithm for clumping was not derived from any model of turbulence, but rather from hierarchically clumped models of the density distributions in the manner described in Mathis, Whitney, & Wood (2002), following Elmegreen (1997). Points were placed within a cube as described below. The cube was partitioned into 65^3 cells, and the final gas density within each of the cells was proportional to the number of points falling within the cell. The exciting star was placed at the center of the cube. Initially 32 points were cast randomly throughout the cube. Surrounding each of these another 32 points were cast randomly within a distance determined by the “fractal dimension”, D , of the model (see Mathis, Whitney, & Wood 2002 for details). Around each of these points another 32 were nested, and finally 32 more around each of the preceding round of casting. Thus, the structure, if it were continued indefinitely, would be considered “fractal”, but the power spectrum is a power law only over about a decade in sizes of projected densities. The mean density was taken to be $n(\text{H}) = 100 \text{ cm}^{-3}$, with a fraction f_{smooth} in a uniform distribution and the rest in the clumped cells. The f_{smooth} represents an average over a still finer distribution of subclumps, not spatially resolved in our simulation, that extend down to very small scales.

For this paper we chose $f_{\text{smooth}} = 0.15$, so the minimum density of a cell is 15 cm^{-3} . The maximum density within these models was 2700 cm^{-3} , with a spread of $\pm 15\%$ arising from different initial seeds. For comparison to the clumped geometries, uniform models were computed with the same stellar luminosity and $n(\text{H}) = 100 \text{ cm}^{-3}$. The uniform models fitted more compactly into the grid cube and consequently could employ a mesh 2.7 times finer than the clumped models. The abundance patterns found with the coarse and finer resolution uniform models are in close agreement except for O^0 (the coarse being 1.5 – 2.2 times larger).

In order to test the effects of allowing radiation to escape from our clumped models through vacuum instead of unresolved cells, we ran models with $f_{\text{smooth}} = 0$. About 10% of the ionizing photons escaped the simulation, as opposed to $\sim 1.5\%$ for the $f_{\text{smooth}} = 0.15$ models.

The distribution of the density in the clumped models is determined by three parameters: (a) f_{smooth} , (b) the initial seed for the random number generator, and (c) the “fractal dimension”, D , that determines the power spectrum of column densities as projected from an assumed cube onto the plane of the sky. We considered $D = 2.6$ and 2.9, and averaged all clumped models among the same five arbitrarily chosen initial seeds. Thus, we have an indication of the dispersion of various physical quantities among clumpy models with the same fractal dimension.

5. The H-ionizing photon luminosity of the exciting star in units of 10^{49} photons s^{-1} , L_{49} , was increased from 0.1 to 100, in steps of factors of ten. For uniform models this is equivalent to changing the “ionization parameter”, $U \equiv 10^{49} L_{49} / (4\pi R_S^2 n_e c)$, by factors of $10^{1/3}$ (R_S is the Strömgren radius and n_e the electron density.) A large U implies large abundances of high stages of ionization and a relatively sharp increase of (H^0/H) near the edge of the Strömgren sphere. In clumped models the ionized region is not spherical and there is no constant value of n_e , but L_{49}

is an equivalent parameter to explore the effects represented by U in uniform models. For instance, our results are applicable to superstar clusters: $L_{49} \sim 10^3 - 10^4$, $n_e \sim 10^3 - 10^4 \text{ cm}^{-3}$ in starburst galaxies.

6. The dielectronic recombination coefficients for sulfur are poorly known. Unfortunately, they can be important for the ionization of S. We followed Ali et al. (1991), using averages of various ions of C, N, and O. We tested the importance of these assumptions by calculating some models with all dielectronic recombinations for S being zero. Of course this is an extreme assumption, since a lack of knowledge of the values of coefficients does not imply that they are zero. We discuss the results in §3.5.4.

The cube for clumped models was large enough so that $\lesssim 1\%$ of the ionizing radiation escaped through the edges. The outer boundaries of the ionized regions were very irregular in shape, and for all stellar temperatures there are a few regions of neutral H and He embedded within the ionized gas, with the gas that they shadow from the star ionized by recombination radiation.

7. Our cell sizes are large in comparison to the mean free paths of ionizing photons when H is almost neutral within the cell. Our code derives a mean ionization for the cell based on the radiation entering it without considering any substructure of the ionization within the cell. Our analysis attributes that ionization to the entire mass of the cell, while only a fraction of the cell’s mass would actually be involved. Near the edge, a few photons can produce ionizations that the code assumes are spread uniformly over the entire cell, with a correspondingly low electron density. Therefore, recombinations are underestimated, and too much mass of ionized material is derived. The principal ions for which this effect occurs are H^+ , N^0 , and O^0 . In our analysis we considered only cells in which the code derived (H^+/H) less than H_{min}^0 , a parameter taken to be 0.25 for the results in this paper. This choice provides roughly an optical depth of unity across our cells, for a typical photon that can reach the edge. We have investigated how these results depend the H_{min}^0 . Uniform models are hardly affected because the area of their almost-neutral H zone is much smaller than clumped models. These show a slow decline in (He^+/H^+) as H_{min}^0 is increased from 0.1 to 0.4, and a more rapid drop from 0.4 to 0.9. The increase of $n(\text{H}^0)/n(\text{H})$ between adjacent cells is typically an order of magnitude when the larger (H^0/H) is 0.4 or more.

We kept the number of cells within the model cube constant and varied the physical length of the cube proportional to $L_{49}^{1/3}$. This makes clumped models with the same initial seed have the same ionization structure in terms of the size of the model cube.

Fig. 1 shows (a; upper left) the clumped gas densities in a typical slice through the plane containing the star; (b; upper right) the fraction of H^0 in the same slice, (c; lower left) the intensities of $\text{H}\alpha$, relative to its maximum intensity, as projected onto the sky (with no foreground extinction), and (d; lower right) the $[\text{N II}]/\text{H}\alpha$ ratio projected onto the sky. The axes are in parsecs for a model with $T^* = 40 \text{ kK}$, $L_{49} = 10$. We see that the density through the midplane is concentrated to the left side, but the projected images, (c) and (d), are more symmetrical because of ionization in the foreground and background planes. The $[\text{N II}]/\text{H}\alpha$ is large

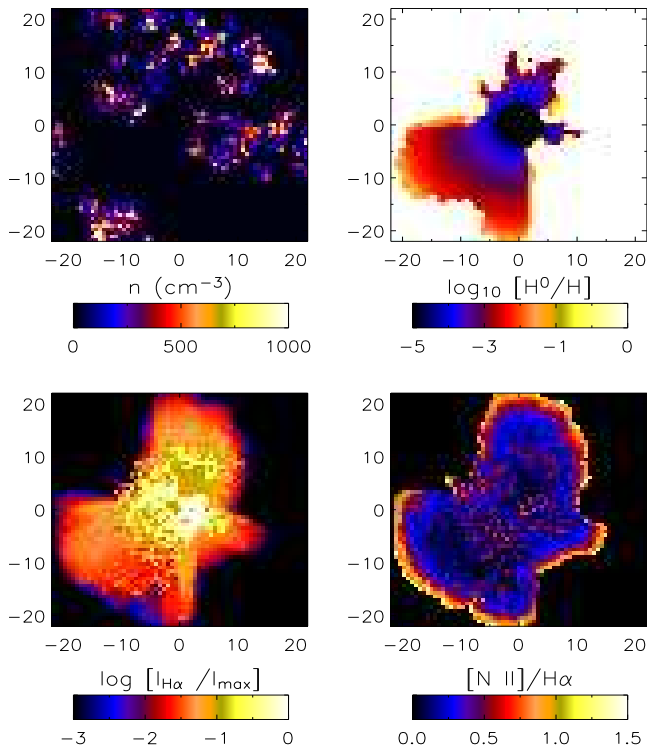


Figure 1. Some properties of the models for $L_{49} = 10$, $T^* = 40$ kK. The axes give distances in parsecs. *Upper left*; A slice through the midplane (containing the star), showing the densities in the models; *upper right*: the fraction of neutral H; *lower left*: a projection of the $H\alpha$ intensity upon the plane of the sky, normalized to the maximum intensity; *lower right*: the projected $[N II]6583/H\alpha$ ratios.

at the edge because the ionization favors N^+ and the temperature is relatively high there.

The large $[N II]/H\alpha$ (lower right panel) at the edges does not imply that the H II region would appear limb-brightened in the sky. The lower left panel shows that the $H\alpha$ intensity at the edges is only $\sim 1\%$ as bright as the maximum, so the $[N II]$ intensity is low and would blend in with the unrelated surrounding diffuse emission. It is only the $[N II]/H\alpha$ ratio that increases at the edges.

3 EFFECTS OF CLUMPING ON IONIC ABUNDANCES

Our results from a large number of models can be summarized simply: for a given exciting star, clumping changes the averaged fraction of ionization of all elements, but differently for relatively cool stars than for hot. The important quantity is $\gamma \equiv (L_{He}/L_H)/(He/H)$. If $\gamma > 1$ a star is “hot”; < 1 , “cool.” Clumping enhances the higher stages of ionization of an element (including He) for cool stars and decreases them for hot. The amounts of enhancement for specific ions are discussed below.

We have $L_{He} = \int L_{\nu}^*/h\nu d\nu$, integrated from the ionization potential of He^0 , $\chi(He^0) = 24.6$ eV, to $\chi(He^+) = 54$ eV. L_H is $\int L_{\nu}^*/h\nu d\nu$, integrated from 13.6 eV to 54 eV.

We count the radiation above 24.6 eV as both H- and He-ionizing because each recombination of He produces about one H-ionizing photon (Osterbrock 1989), so absorptions by He hardly affect the number of H-ionizing photons. Interstellar dust does not affect the distribution of ionization significantly if it contains only silicates, as seems likely (see §2).

3.1 Influences of parameters

There are a large number of parameters in our models. Some set the basic physics and radiative transfer (elemental abundances, T^* , L_{49} , and f_{smooth}), but others are arbitrary: the fractal dimension, D , and the initial seed that determines the density structure in clumped models. The dispersion of the results among the five initial seeds that we arbitrarily chose for each clumped model is not large. Typical variations of (H^+/H) are 0.1%; of (He^0/He) , 0.2% if $(He^0/He) \leq 0.1$ and $< 2\%$ if $(He^0/He) \sim 0.3$. The mean temperatures weighted by $n_e n(H^+)$ vary $\sim 0.5\%$. Varying D from 2.6 to 2.9 produced changes about twice the dispersion among the various seeds of each clumped model. The overall result is that the other parameters were much more influential than D and the initial seed. For the rest of the paper, we will present $D = 2.6$ results as representing clumped models, with results averaged among the five seeds.

We begin by considering the main physical difference between clumped and uniform models, then define averaged abundances for comparing models, and then consider specific elements and ions.

3.2 Propagation of He Ionizing Radiation

The most important consequence of a clumped density distribution is the fate of He ionizing radiation, depending upon the hardness of the stellar radiation. It determines the relative amounts of the nebular opacity supplied by H and He, the two big players for almost all ionizing photons.

Hot stars produce bountiful He-ionizing photons, so H can compete with He for He-ionizing radiation. At $h\nu = 25$ eV, just above $\chi(He^0)$, H contributes $\sim 40\%$ of the opacity near the star with $T^* = 45$ kK, and He practically all of the rest. In a uniform model, the fraction of H opacity gradually falls with distance from the star as He becomes more neutral. In the interclump regions of clumped models, the H opacity decreases less rapidly with distance because the density is lower. The abrupt increase of density when stellar photons encounter a clump makes the increase of He opacity over H occur within a small volume. The overall effect is to make H compete for He-ionizing radiation more effectively in clumped models than in smooth, thereby decreasing (He^+/He) and other high stages of ionization over uniform models.

He supplies 95% of the opacity for 25 eV photons when $T^* = 37.5$ kK. In this case, in clumped models the He is ionized in the interclump medium until the outflowing starlight encounters a clump, at which point both H and He tend to become neutral. In a uniform model, the He goes neutral after it absorbs essentially all of the stellar He-ionizing radiation, and there is a substantial region in which H is still H^+ but He is neutral. The overall effect is that He and H

tend to be both ionized within the same volume in clumped models, so the (He⁺/He) within the ionized region is larger than in uniform models. The same effect applies to other high stages of ionization. *This is the major physical cause of differences between clumpy and smooth models.*

We compared clumped models with those with uniform densities, but the root physical causes of the differences lie in the radial symmetry, not the uniformity, of the uniform models. The general distinctions between clumped and uniform models applies to any smooth distribution of gas density.

We considered Kurucz (1994) stellar atmospheres of (37.5, 40, 42.5, and 45) kK, $\log g = 4$ and used a power-law interpolation between them to estimate spectra for 38.1, 38.7, and 41 kK as well. For these atmospheres, $\gamma = 1$ occurs at about 39.1 kK. We will see qualitative differences in the ionization structure for other elements at this T^* . For Kurucz atmospheres, $\gamma = (0.569, 1.35, 2.41)$ for $T^* = (37.5, 40, 45)$ kK. We present plots of ionization fractions vs. T^* because γ , the real independent variable, is a less familiar quantity.

3.3 Comparing Models with Observables

Our aim is to compare the abundances within our clumped models with the abundances that would be inferred if the emissions from the models, measured without error or dust, were interpreted in the ways used on actual nebulae. The derived abundances differ from the actual ones in the model because of temperature and density variations within the model, even if the density is never enough to de-excite the emission lines by collisions. If there is poor spatial resolution, there is averaging over the face of the nebula as well. We will compare three types of averaged abundances of a particular ion, X^i , relative to H. The line emission (photons $\text{cm}^{-3} \text{s}^{-1} \text{ster}^{-1}$) is $n(X^i)n_e j_\lambda(X^i, T_e)$, and j_λ is presumed to be known from atomic theory.

Since the model provides 3-D ionization structure of the nebula, the true abundances are known:

$$\left(\frac{X^i}{\text{H}^+}\right)_{\text{true}} = \frac{\int n(\text{He}^+) dV}{\int n(\text{H}^+) dV}. \quad (1)$$

An observer would know the projected line intensities, $I_\lambda = \int n(X^i)n_e j_\lambda(X^i, T_e) dz$, where z is the distance along the line of sight, averaged over the observer's spatial resolution. An extreme assumption would be that there is no spatial resolution over the face of the nebula, so that we know only the total line fluxes, F_λ , thereby obtaining a "global" averaged abundance:

$$F_\lambda = \int I_\lambda dx dy, \quad (2)$$

$$= \int n(X^i)n_e j_\lambda(X^i, T) dV. \quad (3)$$

$$\left(\frac{X^i}{\text{H}^+}\right)_{\text{global}} = \frac{F_\lambda(X^i)/j_\lambda(X^i, T_X)}{F(\text{H})/j_\lambda(\text{H}, T_H)} \quad (4)$$

$$= \frac{\int n(X^i) w(X^i) dV}{\int n(\text{H}^+) w(\text{H}) dV}, \quad (5)$$

where T_X is the measured averaged temperature relevant to the ion X^i , depending upon whether it is a high or low stage. The weights $w(X^i) = n_e j_\lambda(X^i, T)$, and similarly for

the H lines. For high ions we use $T([\text{O III}])$, obtained from $[\text{O III}]\lambda 4363/(5007+4859)$. For low ions we use $T([\text{N II}])$, from $[\text{N II}]\lambda 5755/(6583+6548)$.

We will explore the effects of the $w(X^i)$ on the derived abundances. Note that the effect is not limited to variations in temperature: it exists even in artificial isothermal models because of variations in n_e .

Another extreme assumption is that (X^i/H) can be determined at each point (x, y) , and the result, $A_X(x, y)$, then averaged, weighting the bright pixels more than the faint. We define the abundances averaged over the face of the nebula by

$$\left(\frac{X^i}{\text{H}^+}\right)_{\text{ave}} = \frac{\int A_X(x, y) I_H(x, y) dx dy}{\int I_H(x, y) dx dy}. \quad (6)$$

The fluctuations of temperature within our models are modest, as uniform and smooth models have previously suggested. The variation of $T([\text{O III}])$ across the face of a nebula (e.g., O'Dell et al. 2003) is described by $t^2 = \int (T(x, y) - T_0)^2 dx dy / [T_0^2 \int dx dy]$, where $dx dy$ is the element of area on the sky and T_0 is the averaged temperature. O'Dell et al. (2003) found t^2 in the range 0.005 – 0.016 in five regions of the face of the Orion Nebula using HST images of $\lambda 4363$ and 5007 with high spatial resolution. For $T^* = 40\text{kK}$ and $L_{49} = 10$, our models collapsed along one axis yield $t^2 = 0.0012$ for the uniform model and $(1.0-1.6) \times 10^{-3}$ for the clumped models with various initial seeds. For $T^* = 45\text{kK}$, $t^2 \sim 0.002$. Thus, the Orion Nebula shows temperature fluctuations in excess of models, but not enough to explain the discrepancies between collisionally excited and recombination lines unless one assumes that in real nebulae more violent fluctuations are averaged out by the integration along the line of sight.

We do not discuss fine structure lines ($[\text{O III}] 52, 88 \mu\text{m}$, plus several others) because their emissivities are not sensitive to variations in temperature or densities within the rather modest ranges that we consider. These lines provide excellent diagnostics of the true abundances of their respective ions for both clumped and uniform models, but are subject to collisional de-excitations in real objects.

We now discuss individual ions and elemental abundances.

3.4 He⁺/H⁺

Figure 2 displays (He^+/H^+) plotted against T^* for clumped models (upper sets of curves) and $(\text{He}^+/\text{H}^+ - 0.1)$ for uniform density distributions (lower sets). The horizontal lines at $(\text{He}^+/\text{H}^+) = 0.1$ and 0.09 show the cases of complete ionization of He. The solid lines are true abundances (eqn. 1) for $L_{49} = 0.1$; the dashed lines are for $L_{49} = 100$. The dot-dashed lines are the global abundances (that would be deduced by observers using the fluxes of lines) for $L_{49} = 0.1$, the dotted for $L_{49} = 100$. The other values of L_{49} have curves lying between the ones shown. The bends in the curves near $T^* = 39.5\text{kK}$ occur because $\gamma \sim 1$, so that the ratio of stellar ionizing photon luminosities for He and H, $L_{\text{He}}/L_{\text{H}}$ equals the elemental abundance ratio (He/H) .

Fig. 2 shows that clumped models provide a larger He^+/H^+ at a given low T^* than uniform models; ~ 0.06 at $T^* = 37.5\text{kK}$, as opposed to ~ 0.04 for uniform. For hot stars,

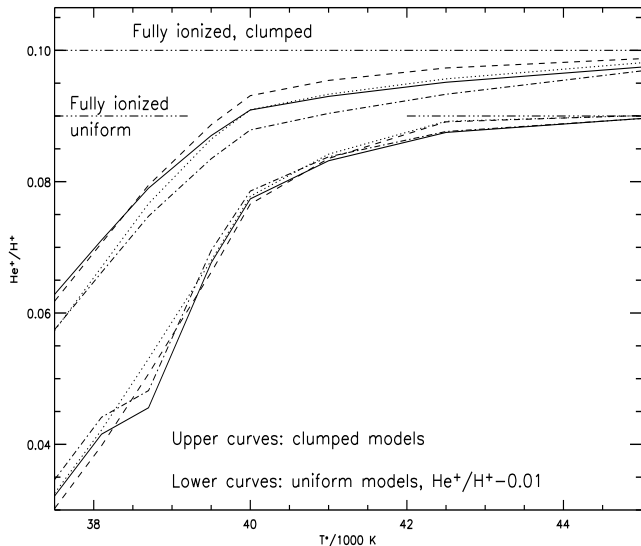


Figure 2. The ratio (He^+/H^+) as determined for clumped (upper set of curves) and uniform models, plotted against the exciting star temperature, T^* . The uniform models show $[(\text{He}^+/\text{H}^+) - 0.01]$. The horizontal lines show complete ionization of He for clumped and uniform models. Solid lines are true abundances (see eqn. 1) for stars with $L_{49} = 10^{-49} L_* = 0.1$; L_* is the ionizing photon luminosity. Dashes: true abundances for $L_{49} = 100$. Dot-dashes: global clumped abundances that would be derived by observers (see eqn. 5) for $L_{49} = 0.1$; dotted, global abundances for $L_{49} = 100$. The ratio of stellar ionizing photon luminosities for He and H, $L_{\text{He}}/L_{\text{H}}$ equals the elemental abundance ratio (He/H) at $T^* = 39.5$ kK, producing the bends in the curves.

the uniform models (the lower set of curves) have $(\text{He}^+/\text{H}^+) = (\text{He}/\text{H})$ to high accuracy, but this is not so for clumped nebulae. They have $\sim 2.5\%$ of He^0 even for $T^* = 45$ kK for the true abundances, and the derived global (He^+/H^+) (i.e., weighted by n_e) is 98.1% of (He/H) . The difference between the derived (He^+/H^+) and (He/H) is 3.8% for 42.5 kK stars. The error increases for lower stellar temperatures and L_{49} .

The relatively large fraction of neutral He for clumpy nebulae surrounding hot stars has important consequences:

(a) (He/H) is a major prediction of Big Bang Nucleosynthesis, and the comparison with real nebulae requires very high accuracy in the correction for He^0 (see Olive & Skillman 2004 for a review showing the accuracy required). The reason why clumped models exhibit more He^0 than uniform models is independent of metallicity. The observations and interpretation of He I emission lines in metal-poor extragalactic H II regions strive for accuracies of $\sim 1\%$ in He^+/H^+ (e.g., Peimbert et al. 2000). There must be corrections for stellar absorption lines underlying the nebular emissions as well as density and temperature effects on the He I line strengths. Uniform or smooth models for nebulae ionized by collections of very hot stars predict that $\text{He}^+/\text{H}^+ = \text{He}/\text{H}$. Clumped models suggest an increase of He/H of the order of $\sim 3\%$ to correct for He^0 . Equation 11 of Olive & Skillman (2004) suggests that uncertainties in the determination of the primordial He^+/H^+ amount to $\sim 10\%$, but the correction for He^0 is systematically upwards.

(b) Helium is dominant in determining the opacity for energetic photons that produce ions of other elements, ex-

ceeding hydrogen by a factor of a few near its ionization edge. For harder radiation ($h\nu > \chi(\text{O}^+) = 35$ eV), its main competitor, O^+ , typically provides $< 30\%$ of the opacity, and the other ions contribute significantly less because of their relatively low elemental abundances. Thus, the increased He^0 decreases the abundances of high stages of ionization of heavy elements.

3.5 Heavy Elements

For heavy elements, the ionic abundances are strongly influenced by whether He recombinations to the ground term, $h\nu \sim 25 - 26$ eV, can ionize the stage in question (e.g., $\chi(\text{S}^+) = 23.3$ eV), so that the He recombination radiation competes with stellar radiation. If the He radiation cannot produce ionization, for cool stars the lower stage (O^+ , Ne^+ , N^+) is reduced in clumped models as compared to uniform. This behavior is similar to He^0 (figure 2) because lower He^0 implies a smaller opacity for hard stellar photons.

There are systematics in the temperatures measured in various ways. For all geometries, $T([\text{O III}])$ is cooler than the n_e -averaged temperature, $\langle T \rangle \equiv \int T n_e dV / \int n_e dV$, by ~ 300 K because O^{+2} is a powerful coolant. $T([\text{N II}])$ is warmer than $\langle T \rangle$ by ~ 400 K because stellar photons are always harder on average at the outer regions of the ionized gas where $[\text{N II}]$ is produced, and O^+ is not as efficient a coolant as O^{+2} . Clumped models have warmer $\langle T \rangle$ than uniform; for $T^* = 37.5$ kK, the difference is 50 – 100 K; for $T^* = 45$ kK, it is ~ 180 K. $T([\text{N II}])$ for uniform models is about 50 K larger than for clumped. These temperature differences affect the derived abundances.

3.5.1 High stages of Ionization: O^{+2} and Ne^{+2}

This section deals with the two ions with very similar behavior as regards differences between uniform and clumped models: O^{+2} and Ne^{+2} . Their important characteristics are that they cannot be ionized by He recombination radiation and cannot be ionized to still higher stages by stellar radiation ($\chi(\text{O}^{+2}) = 54.9$ eV; $\chi(\text{Ne}^{+2}) = 63.4$ eV). This group does not include S^{+2} ($\chi = 34.8$ eV) because it can be ionized to S^{+3} by stellar radiation. We will assume that there are only observations of N^+ optical lines and discuss nitrogen in the next section, although there are fine-structure transitions of N^{+2} at $57 \mu\text{m}$ and of N^{+3} at $69 \mu\text{m}$.

Figure 3 shows (O^{+2}/O) plotted against T^* for both true abundances and the global averages, for $L_{49} = 10$. Heavy lines are clumped models and thin are uniform. The true abundances are solid lines and the global abundances using $T([\text{O III}])$ are dashed.

Figure 4, showing $(\text{Ne}^{+2}/\text{Ne})$, is analogous to Figure 3. The similarities in the ionizations are clear. Ne^{+2} starts lower than O^{+2} at low T^* but increases faster because it requires harder radiation: $\chi(\text{Ne}^+) = 40.96$ eV; $\chi(\text{O}^+) = 35.1$ eV.

Figures 3 and 4 show that:

1. For clumped models the accuracy of the global (O^{+2}/O) abundances derived from $T([\text{O III}])$ is only $\sim 70 - 80\%$ of the true. *Even perfectly accurate $[\text{O III}]$ and $\text{H}\beta$ line intensities do not lead to an accurate determination of O^{+2} abundances.* The reason is that there are relatively strong

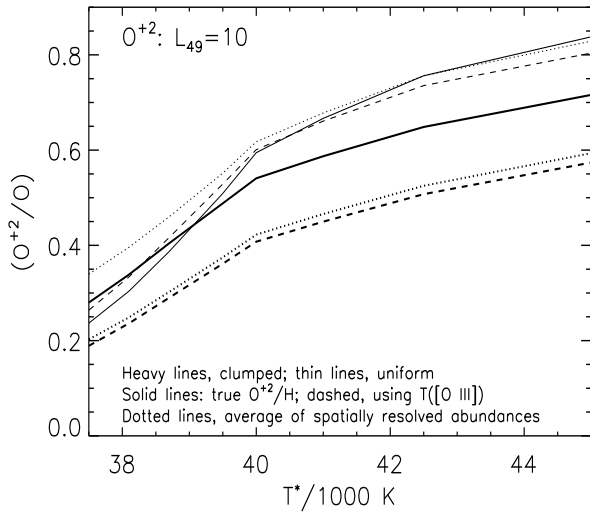


Figure 3. The fraction of oxygen in O^{+2} vs. T^* for L_{49} , the exciting stellar photon luminosity in units of 10^{49} sec^{-1} , =10. The heavy lines are clumped models; the thin lines, uniform. The solid lines are the true abundances; the dashed are derived from $T([\text{O III}])$; the dotted are the spatially resolved abundances, averaged over the face of the nebula (see equation 6.)

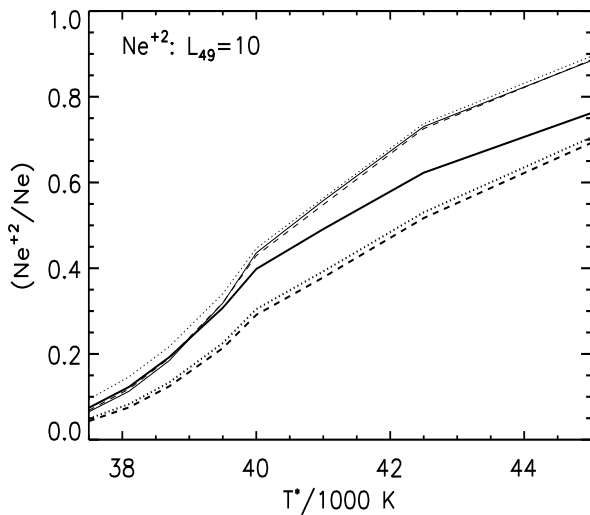


Figure 4. Plots of the $(\text{Ne}^{+2}/\text{Ne})$ ratio, with the same notation as used for figure 3. Note the strong similarities, for reasons discussed in the text.

temperature fluctuations within the O^{+2} zone in clumped models. Excess $[\text{O III}] \lambda 4363$ is produced by the warmer regions, making the mean $T([\text{O III}])$ within the zone higher than the true mean temperature. This situation leads to an erroneously low abundance being determined for O^{+2} . $(\text{Ne}^{+2}/\text{Ne})$ is somewhat more accurately determined than (O^{+2}/O) .

For uniform models, $T([\text{O III}])$ global abundances are in excellent agreement with the true. Surprisingly, the accuracy of the $T([\text{O III}])$ abundances is better for Ne^{+2}

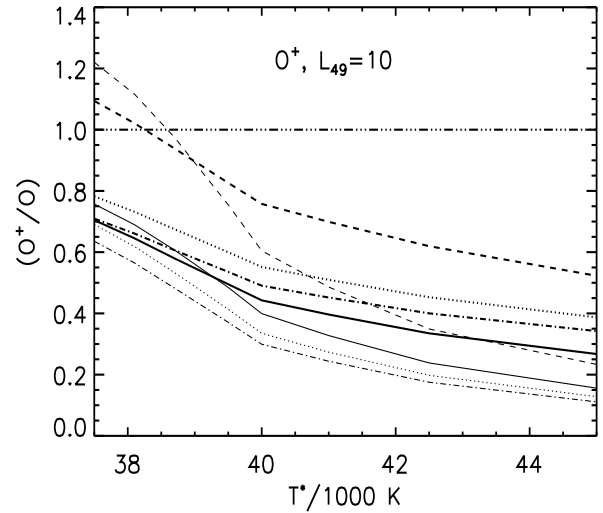


Figure 5. Global (O^+/O) vs. T^* for $L_{49} = 10$. The heavy lines are clumped models; the thin, uniform. The dashed lines are derived from $T([\text{O III}])$; the dot-dashed from $T([\text{N II}])$. The dotted lines are averaged abundances.

than for O^{+2} . For both uniform and clumped models, $(\text{Ne}^{+2}/\text{Ne}) \sim (O^{+2}/O)$ until both are

2. The averaged spatially resolved abundances (dotted lines) are almost the same as those obtained with no spatial resolution.

3. The true (O^{+2}/O) and $(\text{Ne}^{+2}/\text{Ne})$ are larger for clumped models than for uniform in cool stars and smaller for hot stars, as was true for (He^+/H^+) (see Figure 2).

The behavior of (O^{+2}/O) and $(\text{Ne}^{+2}/\text{Ne})$ at other values of L_{49} is as expected. Decreasing L_{49} decreases high stages of ionization: for $L_{49} = 0.1$, the set of curves has the same form as those already plotted but lie entirely under the envelope of the curves shown.

3.5.2 Low Stages of Ionization: O^+ and N^+

These ions and their next higher stages have far larger abundances than the remaining stages of ionization (O^0 , N^0 , and N^{+3}) over the bulk of the nebula. Both O^+ and N^+ are further ionized only by stellar radiation: $\chi(O^+) = 35.12 \text{ eV}$ and $\chi(N^+) = 29.6 \text{ eV}$, well above the energy of almost all He recombinations.

The (O^+/O) global ratios for $L_{49} = 10$ are shown in Figure 5. Heavy lines are clumped models, thin are uniform. Solid lines are true abundances; dashed are global abundances derived from $T([\text{O III}])$ and dot-dashed from $T([\text{N II}])$. The dotted lines are averaged abundances. Figure 6 gives (N^+/N) . Both show that the use of $T([\text{O III}])$ for a low stage of ionization is problematic, especially for cool stars. The $T([\text{N II}])$ abundances for N^+ are $\sim 40\%$ too large but are, surprisingly, more accurate for (O^+/O) than for (N^+/N) .

Using $T([\text{O III}])$ for O^+ and N^+ is especially problematic for clumped nebulae with hot exciting stars; the abundances will likely be overestimated by a factor of ~ 1.5 . Us-

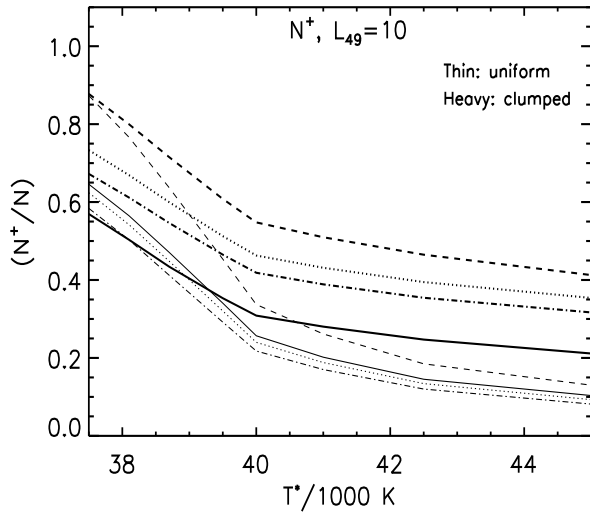


Figure 6. Plots of the N^+ against T^* for $L_{49} = 10$ for clumped models (heavy lines) and uniform models (thin lines). Solid lines are true abundances. Dot-dashes: global abundances derived from $T([\text{N II}])$. Dashes: global abundances using $T([\text{O III}])$. Dots: average abundances (see equation 6).

ing $T([\text{N II}])$ provides results within $\sim 20\%$ of the true for (O^+/O) and $\sim 30\%$ for (N^+/N) .

3.5.3 Neutrals: O^0 and N^0

In regions where these ions are abundant, their ratio to the singly-charged species is almost completely determined by charge exchange with H^0 . $[\text{O I}] \lambda 6300$ emission is produced almost entirely in a physically thin zone at the outer edge of the H^+ zone. In this region there is appreciable H^0 ($\gtrsim 0.5\%$) for charge exchange and a reasonably high T_e , needed to produce the collisional excitation of $[\text{O I}]$. Newly ionized gas flows away from the neutral material, and gas dynamics, neglected in our models, plays an important role in the local temperature and ionization structure. Both the width of the zone affected by dynamics and the mean free path of ionizing photons are less than our cell size, so we resolve this region poorly. We do not present predictions for (O^0/O) , which we find to be $\sim 3\%$ for $L_{49} = 0.1$ and 1% for $L_{49} = 100$. These values are almost surely overestimates. Our (N^0/N) is similarly unreliable. The cells in which $0.25 \leq (\text{H}^+/\text{H}) \leq 0.9$ have a mass of $\sim 8\%$ of the highly ionized plasma in uniform models and $\sim 30\%$ in clumped. However, the temperature in the partially ionized gas is falling rapidly as H^+/H decreases, so the emissions from the almost neutral gas are small. The region $0.9 < (\text{H}^+/\text{H}) < 0.99$ adds only $\sim 1\%$ to the mass and is quite cool (< 6000 K), so it contributes a negligible amount of emission.

3.5.4 Sulfur

Sulfur has four relevant stages of ionization: S^+ ($\chi = 23.3$ eV, so it is ionized by the most energetic He recombination radiation); S^{+2} ($\chi = 34.8$ eV, similar to O^{+2}); S^{+3}

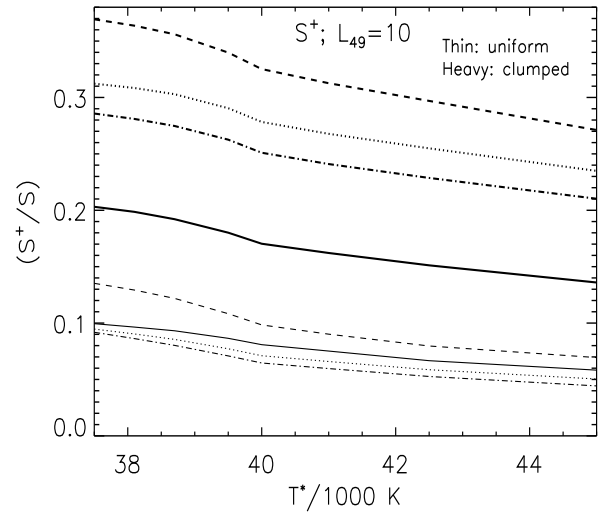


Figure 7. Plots of the (S^+/S) against T^* for $L_{49} = 10$ for clumped models (heavy lines) and uniform models (thin lines). Solid lines are true abundances; dot-dashes, global abundances derived from $T([\text{N II}])$; dashes, global abundances using $T([\text{O III}])$; dots, average abundances (see equation 6). Compared with Figure 5, the same diagram for O^+ , we see the influence of the ionization of S^+ by He recombination radiation that does not affect O^+ .

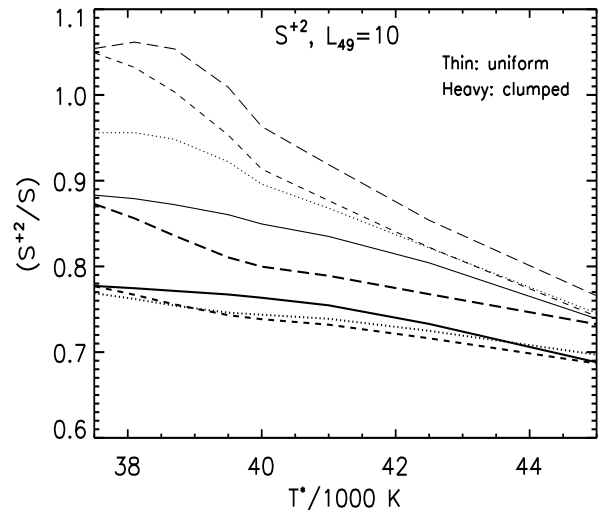


Figure 8. Plots of (S^{+2}/S) against T^* for $L_{49} = 10$ for clumped models (heavy lines) and uniform models (thin lines). Solid lines are true abundances; dashes, global abundances using $T([\text{O III}])$; dots, average abundances (see equation 6).

($\chi = 47.3$ eV), and S^{+4} . There is too little stellar radiation to make S^{+4} important in any of our models.

Figures 7 and 8 show (S^+/S) and (S^{+2}/S) plotted against T^* , both for $L_{49} = 10$. The scheme of the lines is the same as in Figures 3 – 6. These ions do not have the properties of the corresponding stages of oxygen (Figures 3 and 5).

Comparison of Figure 7 with Figure 5 reveals that S^+ has a much smaller true fractional abundance than O^+ because He recombinations ionize S^+ . (S^+/S) varies far less with T^* as well. A greater fraction of O is in O^+ than S in S^+ , so the clumpy nature of clumped models makes more difference for S^+ . The abundance of S^+ in clumped models is three or more times larger than for uniform.

For clumped models, the global abundance of S^+ derived from $T([OIII])$ (the dashed lines in Fig. 7) is about twice the true abundances. The S^+ derived from $T([NII])$ is about 50% too large.

Figure 8 shows the trends of (S^{+2}/S) . The bulk of sulfur is S^{+2} , but both S^+ and S^{+2} decrease with increasing T^* , showing the growing importance of S^{+3} .

The physically implausible assumption that all dielectronic recombination coefficients for S are zero leads to an appreciable shift of the abundances of S ions to the higher stages: from $(S^+ : S^{+2} : S^{+3} : S^{+4}) = (0.172, 0.762, 0.066, 5 \times 10^{-5})$ for $L_{49} = 10$, $T^* = 40$ kK clumped models to $(0.115 : 0.702 : 0.182 : 0.003)$ with no dielectronic recombination for S. Besides the obvious direct consequences for the S line strengths, the averaged electron temperature increases from 8751 K to 8812 K because S^{+2} is a major coolant. However, the effects of geometry, T^* , and L_{49} dominate the effects of the uncertainties in the dielectronic recombination coefficients of S.

3.5.5 Total abundances: O, Ne, and S

Assuming that we have measures of both $T([OIII])$ and $T([NII])$, how well can we estimate total elemental abundances from normally observed emission lines? Oxygen might provide the best case, since all of its ionization stages are observable. We include our estimates of O^0 in our discussion. In a real nebula it would be smaller than our prediction, while O^+ would be correspondingly larger.

Figure 9 shows the estimated global abundances of O, Ne, and S for clumped models, relative to the true abundance. The estimates for oxygen indicate which temperature is used to estimate O^+ and O^0 . $T([OIII])$ is always used for O^{+2} . The estimate for Ne is derived from scaling the Ne^{+2} abundance by the model predictions of (Ne/Ne^{+2}) . The line marked “S(no S^{+3})” simply ignores that ion. The S(ICF) is based on an empirical Ionization Correction Factor (ICF) to account for S^{+3} (Kwitter & Henry 2002). It relates $S/(S^+ + S^{+2})$ to (O/O^+) :

$$S = (S^+ + S^{+2}) \times ICF ; \quad (7)$$

$$\log(ICF) = -0.17 + 0.18\beta - 0.11\beta^2 + 0.072\beta^3 ; \quad (8)$$

$$\beta = \log(O/O^+) . \quad (9)$$

We see that the ICF provides an excellent estimate for the abundance of S.

Figure 10 is similar to Figure 9, except for uniform densities. For clumped models there are compensating errors when we use $T([NII])$ for O^+ and $T([OIII])$ for O^{+2} : the O^+ is too large; the O^{+2} too small. For uniform models, both are only slightly too small. The net result is that the estimated abundance (the dot-dashed lines in figures 10 and 9) is found to be ~ 310 ppm for all T^* and L_{49} , both uniform and clumped. Recall that in our models the true $(O/H) = 330$ ppm.

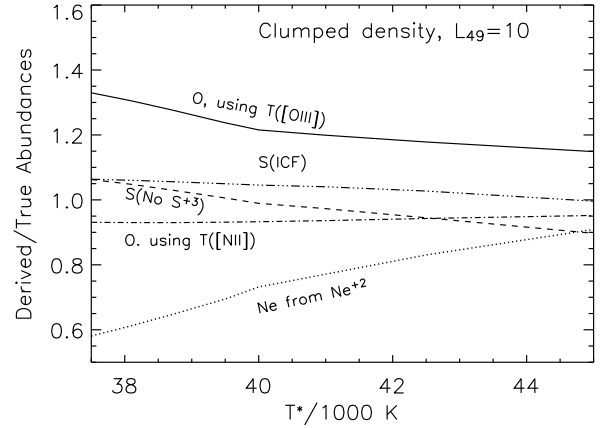


Figure 9. The total estimated global abundances of various elements. The elements and method of estimating its abundance are noted by the lines. For oxygen, “using $T([OIII])$ ” refers to the temperature used for O^+ and O^0 , and similarly for “using $T([NII])$ ”. $T([OIII])$ is always used for O^{+2} . The S(ICF) is from an Ionization Correction Factor to account for S^{+3} (see text).

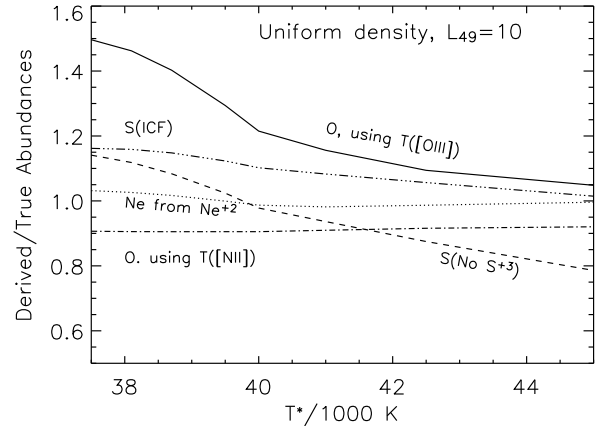


Figure 10. The total estimated global abundances of various elements. The elements and method of estimating its abundance are noted by the lines. For oxygen, “using $T([OIII])$ ” refers to the temperature used for O^+ and O^0 , and similarly for “using $T([NII])$ ”. $T([OIII])$ is always used for O^{+2} . The S(ICF) is from an Ionization Correction Factor to account for S^{+3} .

The importance of being able to use a suitable mean temperature [say, $T([NII])$] for low excitation ions is clear, especially for cool stars. If we are forced to use $T([OIII])$ for O^+ as well as O^{+2} , both estimates are almost always too large (especially for O^+ ; see Fig. 5, dashes). They average about 400 ppm, and the worst (uniform, cool stars, $L_{49} = 100$) is a factor of 1.7 too large. The best case is for uniform geometry models excited by hot stars with $L_{49} = 100$. Its predicted oxygen is almost correct, but the corresponding clumped models predict 20% more than the correct value. Clumping introduces appreciable uncertainties.

The plots of total abundances against T^* for other values of L_{49} are quite similar to those shown in Figures 9 and

10 for $L_{49} = 10$. For $L_{49} = 0.1$, the O using $T([\text{O III}])$ for O^+ (the solid line) is relatively flat at $\sim 120\%$ for both clumped and uniform models, an improvement over the situation at $L_{49} = 10$. For $L_{49} = 1$, the curves are close to those in the figures. The total S without S^{+3} is also better for lower L_{49} , since the levels of high stages of ionization increase with L_{49} . For $L_{49} = 100$, the total S without S^{+3} varies from 110% of the true at $T^* = 37.5$ kK to 83% at 45 kK for clumped and 120% to 66% for uniform models.

4 REMARKS AND SUMMARY

The clumped ionization fractions differ significantly from uniform, and there are significant errors in estimating ionic abundances from emission line fluxes. (He^+/H^+) is significantly increased for cool stars by clumping, and (He^0/He) is appreciable (2 – 3%) for even very hot stars. Clumped models show less (O^{+2}/O) and (Ne^{+2}/Ne) than uniform for hot stars and more for cool. For clumped, the abundances of both ions estimated by the standard methods using emission lines and the appropriate mean temperature, $T([\text{O III}])$, is only $\sim 70\%$ of the true abundances. For uniform models, the derived ionic abundances agree well with true. Real nebulae probably show the same phenomenon, and no improvement in spatial resolution will resolve it.

The strong effects of clumping on ionic abundances for a given stellar energy distribution (§3.5) makes the determination of the properties of the exciting star from the nebular ionic ratios even more problematic than it is with smooth models. Another uncertainty is the presence of carbonaceous dust, with a strong absorption at ~ 17 eV (§2), that makes the spectrum of the exciting star appear hotter because H-ionizing radiation is absorbed more readily than He-ionizing. Silicate dust makes little difference to H II regions because it has a low, almost wavelength-independent cross section.

Real H II regions have irregular outer boundaries if they are bounded by ionization fronts. By means of models with clumped density distributions, we have investigated the effects of the complex shapes of the outer boundary on the analysis of ionic and elemental abundances. We feel that our models contain the elements of a basic physical effect that pertains to real H II regions in all of their geometrical complexities: their boundaries are also complex in shape, more so than our models.

We considered Kurucz (1994) stellar temperatures in the range 37.5 kK – 45 kK and ionizing photon luminosities of $10^{48} - 10^{51} \text{ s}^{-1}$, all for an averaged density of 100 cm^{-3} . Of course, other models of stellar atmospheres have been proposed. The most important parameter of any of them is γ , the ratio of He-ionizing photons to H-ionizing. We considered γ in the range 0.57 – 2.4. Our results apply rather well for densities $n < 10^4 \text{ cm}^{-3}$ to objects with the same L_{49}/n as our models. With our limited spatial resolution we found no regions truly shadowed from the central star. Clumping makes significant differences on the true abundances of ions of N, O, Ne, and S, as well as those derived from emission lines plus measured nebular temperatures, $T([\text{O III}])$ and $T([\text{N II}])$. We considered two extreme limits of spatial resolution: either none, so that only the fluxes of the emission lines were used, or averaging the abundances as determined pixel-by-pixel over the face of the nebula. There

were no major differences introduced by the two methods of averaging.

If $T([\text{N II}])$ is available for analyzing the low stages of ionization, the overall abundances of O, Ne, and S are reasonably accurate because of partially compensating errors. For cool stars (for which most Ne is Ne^+) in clumped models, (Ne/H) is badly estimated from $[\text{Ne III}]$ optical lines. All of these elements are well estimated for uniform models. However, using $T([\text{O III}])$ for both low and high stages of ionization leads to overestimates of (O/H) of $\sim 40 - 60\%$ for both clumped and uniform models, for cool stars.

The underlying physical cause of the differences between clumped and uniform models is the flow of He recombination radiation from zones of high ionization of H that can be in physical proximity to regions near the outer edge of the nebula, with relatively large amounts of H^0 . We discuss this effect in §3.1 and for each ion.

JSM acknowledges support from a PPARC Short Term Visiting Fellowship to St Andrews, and KW from a PPARC Advanced Fellowship. Many of the models were produced with computing facilities granted to Prof. Ellen Zweibel by the Graduate School of the University of Wisconsin-Madison. The comments of an anonymous referee improved the paper.

REFERENCES

- Ackerman, C. J., Carigi, L., Nissen, P. E., Pettini, M., & Asplund, M., 2004, *A&A*, 414, 931
- Ali, B., Blum, R. D., Bumgardner, T. E., Cranmer, S. R., Ferland, G. J., Haefner, R. I., & Tiede, G. P., 1991, *PASP*, 103, 1182
- Asplund, M., Grevesse, N., Sauval, A. J., Allende Prieto, C., & Blomme, R., 2005, *A&A*, 431, 693
- Draine, B. T., 2004, web page at www.astro.princeton.edu/~draine
- Elmegreen, B., 1997, *ApJ*, 477, 196
- Esteban, C., Peimbert, M., Torres-Peimbert, S., García-Rojas, J., Ruiz, M. T., & Rodríguez, M., 1999, *ApJS*, 120, 113
- Esteban, C., Peimbert, M., Torres-Peimbert, S., & García-Rojas, J., 1999, *Rev. Mex. Astron. Astrof.*, 35, 65
- Esteban, C., Peimbert, M., García-Rojas, J., Ruiz, M. T., Peimbert, A., & Rodríguez, M., 2004, *MNRAS*, 355, 229
- Esteban, C., García-Rojas, J., Peimbert, M., Peimbert, A., Ruiz, M. T., Rodríguez, M., & Carigi, L., 2005, *A&A*, 431, 693
- Ferland, G. J., et al., 1995, in Williams, R., Livio, M., eds., *STScI Symp. 8, "The Analysis of Emission Lines"*, Cambridge Univ. Press, Cambridge, 83
- García-Rojas, J., Esteban, C., Peimbert, M., Rodríguez, M., Ruiz, M. T., & Peimbert, A., 2004, *ApJS*, 153, 501
- Grevesse, N., & Sauval, A. J., 1998, *Sp. Sci. Rev.*, 85, 161
- Holweger, H., 2001, in Joint SOHO/ACE workshop "Solar and Galactic Composition". Edited by Robert F. Wimmer-Schweingruber. Publisher: American Institute of Physics Conference proceedings vol. 598
- Howk, J. C., & Savage, B. D., 1999, *ApJ*, 517, 746
- Johnson, K. E., & Kobulnicki, H. A., 2003, *ApJ*, 597, 923
- Kurucz, R. L., 1994, CD-Rom 19, Solar Abundance Model Atmospheres

- Kwitter, K. B., & Henry, R. B. C., 2001, *ApJ*, 562, 804
- Lagache, g., Haffner, L. M., Reynolds, R. J., & Tufte, S. L., 2000, *A&A*, 354,247
- Mac Low, M.-M., 2004, *ApSS*. 289, 323
- MacLow, M.-M., & Klessen, R. S., 2004, *Rev. Modern Physics*, 76, 125
- Mathis, J. S., Whitney, B. A., & Wood, K., 2002, *ApJ*, 574, 812
- O'Dell, C. R., Peimbert, M., & Peimbert, A., 2003, *AJ*, 125, 2590
- Olive, K. A., & Skillman, E. D., 2004, *ApJ*, 617, 290
- Osterbrock, D. E., 1989, *Astrophysics of Gaseous Nebulae and active Galactic Nuclei*, University Science Books, Mill Valley, CA
- Pagel, B. E. J., & Tautvaišienė, G., 1995, *MNRAS*, 276, 505
- Peimbert, M., Peimbert, A., & Ruiz, M.-T., 2000, *ApJ*, 541, 688
- Péquignot, D., et al., 2001, in "Spectroscopic Challenges of Photoionized Plasmas", G. Ferland & D. W. Savin, eds., ASP Conference Series 247. San Francisco: ASP, 533
- Savage, B. D., & Sembach, K. R., 1996, *ARAA*, 34, 279
- Sellgren, K., Tokunaga, A./ T., & Nakada, Y., 2004, *ApJ*, 349, 120
- Sofia, U. J., Laroesch, J. T., Meyer, D., & Cartledge, S. I. B., 2004, *ApJ*, 605, 272
- Tsamis, Y. G., Barlow, M. J., Liu, X.-W., Danziger, I. J., & Storey, P. J., 2003, *MNRAS*, 338,687
- Weingartner, J. C., & Draine, B. T., 2001, *ApJ*, 548, 296
- Wood, K., Mathis, J. S., & Ercolano, B., 2004, *MNRAS*, 348, 1337
- Zubko, V. Dwek, E., & Arendt, R. G., 2004, *ApJS*, 152, 211